Photochemistry and Photobiology, 2014, 90: 1119–1125

"Pointsource" Delivery of a Photosensitizer Drug and Singlet Oxygen: Eradication of Glioma Cells *In Vitro*

Ashwini A. Ghogare[1], Imran Rizvi[2], Tayyaba Hasan*[2] and Alexander Greer*[1]

[1]Department of Chemistry, Graduate Center, City University of New York, Brooklyn College, Brooklyn, New York
[2]Wellman Center for Photomedicine, Massachusetts General Hospital and Harvard Medical School, Boston, Massachusetts

Received 21 February 2014, accepted 18 March 2014, DOI: 10.1111/php.12274

ABSTRACT

We describe a pointsource sensitizer-tipped microoptic device for the eradication of glioma U87 cells. The device has a mesoporous fluorinated silica tip which emits singlet oxygen molecules and small quantities of pheophorbide sensitizer for additional production of singlet oxygen in the immediate vicinity. The results show that the device surges in sensitizer release and photokilling with higher rates about midway through the reaction. This was attributed to a self-amplified autocatalytic reaction where released sensitizer in the extracellular matrix provides positive feedback to assist in the release of additional sensitizer. The photokilling of the glioma cells was analyzed by global toxicity and live/dead assays, where a killing radius around the tip with ~0.3 mm precision was achieved. The implication of these results for a new PDT tool of hard-to-resect tumors, *e.g.* in the brain, is discussed.

INTRODUCTION

There are examples of sensitizers conjugated to compounds or nanoparticles that lead to improved photodynamic therapy (PDT) results (1–6). Sensitizer conjugation to, for example, metal particles or silica have been seen to increase PDT efficiency (7,8) and singlet oxygen production (9–13). Common PDT techniques (14) systemically administer the sensitizer relying on homing to the appropriate site, but attention could be focused on "pointsource" administration techniques as distinct from topical administration.

We describe a pointsource microoptic device that photoreleases sensitizer and emits $^1O_2$ from a silica probe tip (Fig. 1). The device is used here to kill glioblastoma cells where pheophorbide molecules readily cleave off of the probe tip by oxidation of the ethene linker (Fig. 1b,c) (15). Such oxidation processes resulting in bond cleavage (16) based on singlet oxygen chemistry (17–20) have been of interest to us.

Our interests are also in adsorption reactions that participate on silica surfaces. In recent work, we developed surface coatings (designed as a repellent fluorosilane probe surface) for enhanced pheophorbide photorelease of up to 99% of the ethane bonds broken in toluene (21). This fluorinated silica surface was also used for sensitizer drug release and photokilling of ovarian cancer (OVCAR-5) cells—providing initial estimates the device may function as a PDT implement (22).

Based on recent work (21,22), we sought to answer chemical and biological questions in the drug photorelease process. For example, can we explain mechanisms of sensitizer uptake into the cells and the precision of killing when the probe tip is placed in U87 monolayers? Our reasons for pursuing this work are (1) to address significant challenges in the clinic in removing cancers to minimize damage to normal tissue (23,24), and (2) to identify potential benefits of the pointsource approach over conventional systemic photosensitizer delivery, particularly for PDT in the brain, where sensitizer delivery is problematic due to the blood–brain barrier. Here, we describe detailed studies of the pointsource PDT technique, using principles of organic chemistry and photobiology for a basic understanding of interfacial phenomena for sensitizer-photorelease control and cell-killing precision.

In one respect, our work bears similarity to an optical fiber system developed by Kandler *et al.* (25) which is ideal for cultured neurons and brain slices containing caged reagents for photo*un*caging reactions where the light spot is focused.

MATERIALS AND METHODS

Materials. Sterile DMSO, chloroform, hydrofluoric acid and propidium iodide solution (1 mg mL^{-1} in water, dead cell stain) were purchased from Sigma Aldrich (St. Louis, MO). Calcein AM (live cell stain), fetal bovine serum (FBS) and the MTT reagent were purchased from Life Technologies (Carlsbad, CA). Pyropheophorbide-*a* was purchased from Frontier Scientific (Logan, UT). Aqueous-based tissue solubilizer solution was purchased from PerkinElmer (Waltham, MA). Pierce® BCA protein assay kit was purchased from Thermo Scientific (Rockford, IL). Minimum Essential Medium Eagle (Mod.) 1× (MEM), Dulbecco's Phosphate-buffered salt solution (PBS) and 5000 I.U. mL^{-1} penicillin/streptomycin and 50-mg mL^{-1} streptomycin were purchased from Mediatech (Herndon, VA). U87 MG ATCC® HTB-14™ cells were purchased from ATCC (Manassas, VA). To make complete MEM growth media, 1% (*v/v*) 5000 I.U. mL^{-1} penicillin/streptomycin and 50 mg mL^{-1} streptomycin and 10% (*v/v*) FBS was added to a 500 mL bottle of MEM media. Cell culture glass bottom dishes (29 mm glass well size and 14 mm microwell) and #1 cover glass (0.13–0.16 mm) were purchased from *In Vitro* Scientific (Sunnyvale, CA). Falcon 35 mm cell culture dishes and 24-well cell culture plates were purchased from Becton Dickinson Labware (Franklin Lakes, NJ). Corning's code 7930 porous Vycor glass (PVG) was purchased from Advanced Glass and Ceramics (Holden, MA).

Device fabrication and instruments. We have used this device previously (22). A 3 ft long fiber optic was purchased from Fiberoptic Systems, Inc. (Simi Valley, CA). It had an internal 1.1 mm diameter Teflon

*Corresponding authors e-mail: agreer@brooklyn.cuny.edu (Alexander Greer); thasan@partners.org (Tayyaba Hasan)

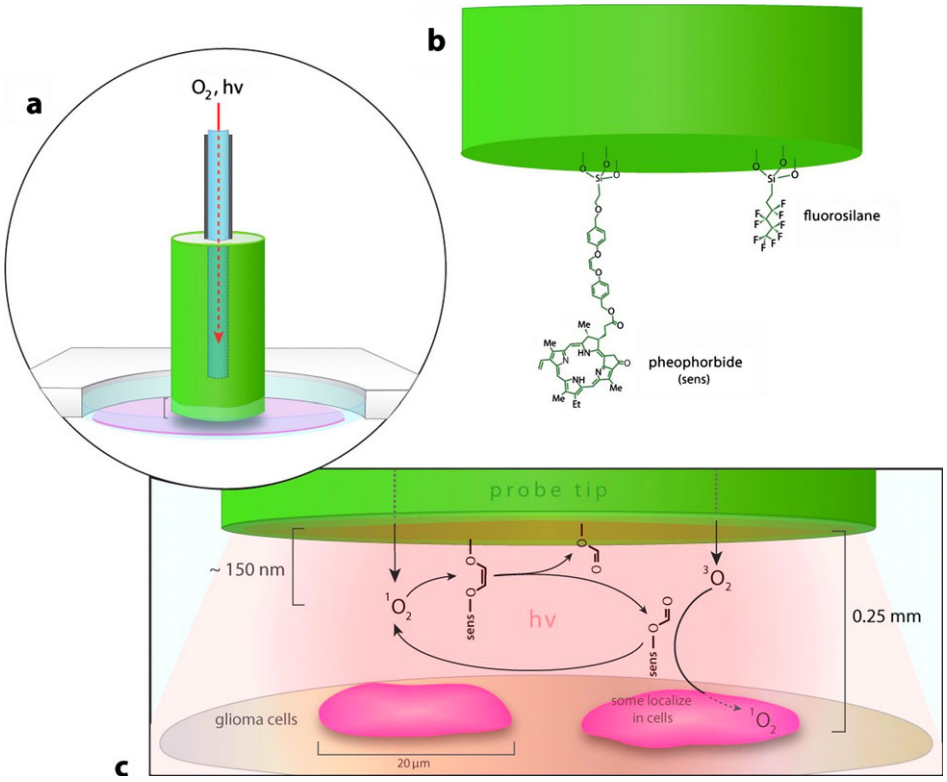

Figure 1. Pointsource device for targeted singlet oxygen delivery: (a) Red laser light and oxygen gas traveled through the hollow fiber optic and emerged from the probe tip. We used 200 mW output from a 669 nm laser and a O_2 gas flow rate of ~0.2 ppm min^{-1} through the probe tip. The probe tip was held vertically in a perpendicular orientation above the cells so as not to kill them by mechanical action. (b) The fiber is equipped with a 5 × 10 mm^2 ($d \times l$) pheophorbide-modified silica tip with a photocleavable ethene linker. The probe design includes a covalently bound nonafluorosilane to improve sensitizer photorelease into the surrounding medium. (c) A view of the singlet oxygen-generating probe tip is shown with sensitizer photorelease and factors that relate to the glioma cell killing mechanism. The sensitizer traverses a relatively long 0.25 mm distance, which stands in contrast to the short ~150 nm diffusion distance of $^1O_2$ in H_2O. The sensitized production of $^1O_2$ also occurs away from the probe tip through diffusion of the pheophorbide via light and O_2 delivered from the probe tip.

gas flow tube from the distal end to a T-valve that was surrounded by excitation fibers, as well as a 1.4 mm diameter black polyvinyl chloride jacket. The Vycor was shaped into cylindrical pieces 5 × 10 mm^2 ($d \times l$) with a Buehler IsoMet Low Speed Saw (Model 11-1280-160), a Buehler ultrasonic disk cutter (Model 170) and a Buehler variable speed grinder-polisher. A hole 1.5 × 7.0 mm^2 ($d \times l$) was bored into the glass pieces with a dremel drill (Model 200) to fit to the fiber optic and was glued in place with ethyl cyanoacrylate. The synthesis of the pheophorbide-modified probe tips was carried out using a procedure as described previously (15,26). The amount of sensitizer covalently bonded to the probe tips was obtained to be 70 nmol. The diameter of the sensitizer molecule is ~20 Å and pore sizes in the silica are ~40 Å. The penetration depth of the sensitizer is 0.08 mm along the outer faces of the probe tip. Light was delivered from a 669 nm CW diode laser (model 7404, 700 mW, 4.1 A output, Intense Inc., North Brunswick, NJ) that was connected to the optical fiber and the power (1 W cm^{-2}, spot size 0.196 cm^2) was determined with a VEGA Laser Power Energy Meter (Ophir Laser Measurement Group, LLC, North Logan, UT). With the optical fiber pinned to a translation stage (OptoSigma Corp., Santa Ana, CA) for ±0.1 mm precision movement, the diode laser was connected to its proximal end through an SMA connector. Based on a previous report (27), the O_2 gas flow rate through the probe tip was ~0.2 ppm min^{-1} as measured by a Clarke-type oxygen electrode. The amount of sensitizer covalently attached was determined by monitoring its Soret absorption (λ = 415 nm) after liberation from unused probe tips on dissolution with 40% (*v*/*v*) aqueous hydrofluoric acid and extraction with chloroform. The total amount of sensitizer remaining on the probe tip after photorelease was measured in terms of mV using a Labsphere integrating sphere (North Sutton, NH) attached to a Fluke 79 Series II Digital Multimeter (John Fluke Mfg. Co., Vail, AZ). The multimeter was calibrated prior to use and the amount of covalently bound and adsorbed sensitizer were obtained from calibration curves. Fluorescence measurements were made with a SpectraMax M5 Multi-Mode Microplate Reader from Molecular Devices (Sunnyvale, CA). Absorbance measurements were made with an Evolution 300 UV–Vis Spectrophotometer (Thermo Fisher Scientific, Franklin, MA).

Sensitizer photorelease in phosphate-buffered saline. Oxygen gas and 669 nm excitation light, intensity of 1 W cm^{-2} (measured with fiber, without cap) were delivered for 2 h, through the fiber optic to probe tip loaded with covalently bound sensitizer dipped in a 200 µL PBS solution. From the photocleaved pheophorbide PBS solution, 50 µL was sampled out at 0.5, 1, 1.5 and 2 h periods and diluted with 50 µL DMSO to measure fluorescence of the sensitizer. The photocleavage of sensitizer away from the probe tip was followed by fluorescence in solution (λ_{ex} = 405 nm, λ_{em} = 675 nm) using the plate reader. The concentration of photosensitizer was obtained from the preconstructed calibration curves of pheophorbide in (1:1) (*v*/*v*) DMSO:PBS solution. The amount of pheophorbide photoreleased was calculated as follows: % photorelease = [(photorelease/loading per area)] × 100. A 1/10th portion of the cap was dipped in 200 µL PBS solution and the quantity of dye that photocleaved was based on the amount of sensitizer covalently attached (7 nmol) to the front face of the cap (20 mm^2 area). The amount of sensitizer adsorbed was measured by soaking the cap in 1 mL *n*-butanol solution for 24 h followed by fluorescence measurements using the plate reader.

Cellular uptake in U87 MG cell monolayer. Human brain carcinoma cells (U87 MG) were maintained in complete MEM growth media at 37°C in a 5% CO_2 incubator. U87 cells (100 000 per well) were seeded in a 24-well cell culture treated plate and maintained at 37°C in the 5% CO_2 incubator. Twenty-four hours later, 0.20 mL volume of MEM media (without phenol red) containing concentrations of pyropheophorebide-*a* ranging from 0.025 to 2.5 µM in 1% (*v*/*v*) DMSO was added to the cells

under subdued light conditions. The cells were incubated with the pyropheophorebide-*a* containing media for times ranging from 0.5 to 2 h. At each time point, the 0.20 mL of the supernatant media was removed from each well and diluted with 0.20 mL DMSO to determine the amount of pheophorbide remaining in the media by fluorescence using a microplate reader. The pheophorbide taken up and associated with the membrane of the U87 MG cells was extracted in 200 μL of the tissue solubilizer solution by digesting the cells for 30 min and the concentration of pheophorbide in the cell lysates was measured by fluorescence. Intracellular and bound concentrations of pheophorbide were quantified from preconstructed calibration curves of known concentration range of pheophorbide in cell lysates. The total protein content of the cell lysates was determined using the BCA protein assay kit, and calibration curves prepared from known concentrations of BSA in the tissue solubilizer solution.

Phototoxicity of pyropheoporbide-a in U87 MG cell monolayer. U87 cells (210 000 per well) were plated in a 35 mm cell culture dish in complete MEM media and maintained at 37°C in a 5% CO_2 incubator for 24 h. A concentration range of pyropheophorbide-*a* in 1.0 mL MEM media (0.025–2.5 μM) was added to U87 cell monolayer. Immediately after addition of the media containing pheophorbide, the cells were treated with the device fitted with a "bare" tip at 669 nm laser, 150 mW cm^{-2} intensity and continuous oxygen sparging for 0.5 or 1.0 h. Control conditions such as "no treatment," "light only" and "dark control" containing 2.5 μM pheophorbide were also done to ensure the reliability of the data. Postdevice treatment, the media containing pheophorbide were aspirated and fresh complete growth MEM media were added to each treatment and control dish, and maintained at 37°C in a 5% CO_2 incubator. Next day, cell viability was measured by assay (28) and the surviving fraction was normalized to the "no treatment" controls.

Treatment procedure. U87 cells (170 000 per well) were plated in 29 mm glass bottom cell culture dish with 14 mm glass bottom microwell insert, in complete MEM media and maintained at 37°C in a 5% CO_2 incubator. Before treatment, media were aspirated and 0.20 mL complete growth MEM media with 1% (*v/v*) DMSO were added to the cell culture dish. The probe tip loaded with covalently bound sensitizer was placed 0.25 mm above the cells. Device treatment was carried out for 0.5 to 2 h periods with 669 nm light with an intensity of 1 W cm^{-2} (measured with fiber, without cap) with continuous oxygen sparging, as "treatment" groups. Controls such as "no treatment" control, "light only" control with the bare tip and pheophorbide-loaded "tip only" control were done to evaluate the toxicity coming from only light or 1% (*v/v*) DMSO in MEM media. Postdevice treatment, DMSO-containing MEM media were removed, complete growth MEM media were replenished in their place and cells were maintained at 37°C in 5% CO_2 incubator. To determine phototoxicity after 24 h, the media were removed from the cells, the cells were washed with PBS solution and then incubated for 30 min in a live/dead assay made of 0.001% (*v/v*) Calcein AM (live cell stain) and 0.002% (*v/v*) propidium iodide (dead cell stain) in PBS. The confocal fluorescence images of the stained cells were taken on the Olympus FV-1000 confocal using a 10× objective for the entire 14 mm glass microwell. The 488 nm line from an Argon ion laser with paired with a FITC filter set and a 559 nm diode source paired with a TRITC filter set were used to detect cleaved Calcein to label live cells. Cell viability was quantified from the fluorescence images using Image J software, where the surviving fraction was normalized to "no treatment" controls. Importantly, the red fluorescence was lowered due to the loss of detached cells during treatment and washing steps prior to imaging. However, this did not impact the analysis because cell viability was measured using Calcein AM (green fluorescence).

Sources of error. Errors arise from the following sources: (1) volumes were recorded by drawing the media up into a 250 μL Hamilton syringe (±5 μL resolution; equates to 2.5% error). (2) Media evaporation took place (*e.g.* tens of microliters could be lost over the course of the experiment). However, media were added every 30 min to account for this to maintain the volume at 200 μL. (3) The concentration of the pheophorbide in the PBS was based on its fluorescence via its extinction coefficient (accuracy ±0.1 μM). (4) The diameter of the light spot that emerged from the tip was measured with a ruler. It was 0.196 cm^2 viewed by eye (accuracy ~20%). The measurement of the fluence (mW cm^{-2}) of light had an error of ~1%. (5) The normalized cell viability was calculated as the relative absorbance of the MTT reagent using the plate reader. The procedure of incubation with MTT reagent and extraction with DMSO, pipetting out 200 μL sample for absorbance introduces error of 2–5% in the cell viability calculation. (6) The radius of photoxicity was measured using the same protocol described in the "Treatment Procedure" section, using the Image J software "circle tool" option which introduced a ~1% error.

RESULTS AND DISCUSSION

Cell phototoxicity and sensitizer uptake

Initially, we carried out control experiments to find conditions for efficient cell killing. Figure 2 (light bars) shows the percent U87 cell viability, but with a device probe tip that was devoid of any sensitizer molecules. Here, pyropheophorbide-*a* spiked into U87 cell samples followed by light and oxygen from the device tip was used as a control. The U87 cell viabilities were analyzed 24 h post treatment with a 3-(4,5-dimethylthiazol-2-yl)-2,5-diphenyltetrazolium bromide (MTT) assay. These controls demonstrate that greater than 90% cell killing is achievable with 0.5 μM pheophorbide after 1 h. The cell viability decreases as we add higher pyropheophorbide-*a* concentrations due to greater concentrations of $^1O_2$. Our control experiments also demonstrate that the pyropheophorbide-*a* toxicity in the dark is minimal (*i.e.* 0–3% for 0.025–1.0 μM pheophorbide and 4% for 2.5 μM pheophorbide). Evidence for a photosensitized oxidation process is that in the absence of sensitizer, light, or O_2 the cell viability was ~97%. In the absence of sensitizer, but the presence of light and O_2 for 1 h the cell viability was 92–94%.

Figure 2 (dark bars) shows the concentration of pheophorbide that was taken up by U87 cells in MEM media. The dose of pheophorbide added to the cells ranged from 0.025 to 2.5 μM, which corresponded to cellular uptake ranging from 3.6 pmol/μg/mL protein to 252.3 pmol/μg/mL protein. Despite the difference in the amounts of pheophorbide introduced, over 1 h the quantity of pheophorbide taken up was relatively fixed 15–24%, where the uptake appeared to be a linear relationship over this concentration range (slope = 0.152; R^2 = 0.9977).

The data from Fig. 2 taken together point to a 92% cytotoxic response for the delivery of 0.5 μM and uptake of 51.7 pmol/μg/mL

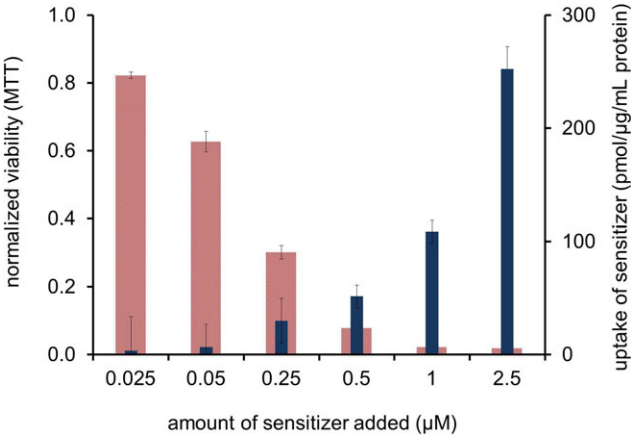

Figure 2. Comparison of sensitizer uptake efficiency in the dark after 1 h (dark bars) with phototoxicity effects on U87 cells treated by a bare-tipped device devoid of sensitizer, but sparging O_2 with red light irradiation with externally added pheophorbide (light bars). Cells were digested for the uptake measurements. Cell viability was assessed by MTT assay and results are shown as normalized relative to control cells. Each value represents an average of two or more experiments.

protein uptake of pheophorbide after 1 h. Although the porous silica probe tip readily loads different amounts of pheophorbide, the information in Fig. 2 helped us identify release quantities that achieve good-level killing.

Course of the sensitizer drug photorelease in phosphate-buffered saline

We have used a probe tip with 7-nmol pheophorbide covalently bound to the working front face. Figure 3 shows the percent of sensitizer photoreleased from the probe tip into 0.20 mL PBS. The plot shows a sigmoidal photorelease behavior. From 0 to 30 min, the photorelease was slow and was then followed by rapid photorelease. After 1.5 h, there was a deceleration. After 2 h, we found that ~10% of the sensitizer had departed from the probe tip, although most of the ethene bonds were consumed (92–95%). The amount of sensitizer adsorbed on the tip was 82 ± 3% based on solvent washes with DMSO and *n*-butanol. This can be understood in terms of limited solubility of the sensitizer in PBS, thereby increasing its tendency to adsorb to the fluorinated silica probe surface.

We (26) previously showed that externally irradiated silica-conjugated sensitizer samples also produce a sigmoidal photorelease in *n*-butanol. There was a kinetic likeness in the photorelease although the sigmoid was 7.7-fold steeper in the *n*-butanol than the PBS. Silica surface properties (29–34) and factors including greater solubility in *n*-butanol than PBS play key roles in the extent of the pheophorbide retention on the silica tip surface. The results were similar from internal irradiation (described here) *vs* external irradiation (26) of the sensitizer solid, where increasing light intensity in the former was a correlation with, but not causation of the sigmoidal behavior.

As might have been expected, the light intensity emerging through the tip increased over the course of the PBS experiment. Power meter measurements have correlated the amount of light delivered through the tip with the fraction of detached sensitizer. Figure 3 shows that after 2 h, there is a net 10% sensitizer photorelease, which only yielded a 23% increase in the light intensity through the probe tip. With the increased light delivery, the affect may be one of increasing the $^1O_2$ concentration available at the end of the fiber adjacent to the probe tip. But we did not attribute the increasing light intensity as playing a significant role in causing the sigmoidal photorelease behavior.

Guided by the results of the microtipped device for sensitizer photorelease in PBS, we proceeded to investigate the efficiency of the pointsource device for killing glioma cells *in vitro*.

Fiber tip-guided sensitizer delivery for cell killing in discrete locations

We have used the device to demonstrate sensitizer photorelease and global phototoxicity to U87 cells in MEM media. The device contained pheophorbide-attached probe tips, and cell viability was measured 24 h after device treatment by live/dead assay and fluorescence microscopy. Here, the phototoxicity was evaluated in 14 mm diameter microwell experiments.

Figure 4 shows a sigmoidal behavior for the photokilling, analogous to the photorelease behavior in solution (Fig. 3). From 0 to 30 min, the cell killing was slow which was followed by an acceleration and then deceleration at 1.5 h. The increasing sensitizer release and light intensity emerging through the tip over the course of the experiment was roughly proportional to the photokilling (inversely proportional to the normalized viability by live/dead assay). The phototoxicity reached a maximum of 79% after 2 h (Fig. 4). We did not observe 100% killing under our experimental conditions.

"Lengthening" the toxic radius of $^1O_2$

Although the diffusion distance of $^1O_2$ is short (35,36) with toxicity that does not extend much beyond ~100 nm (37–39) sensitizer release from our device gives a diffusible photocatalyst that effectively increases it. This was shown in our examination of

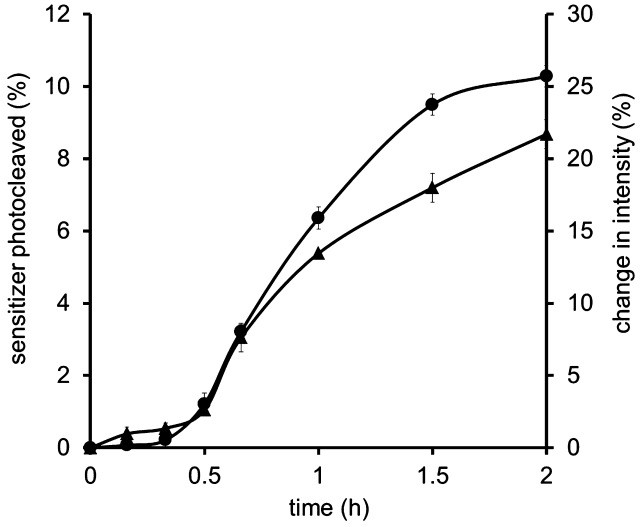

Figure 3. A time-sequence analysis of pheophorbide photoreleased free from the probe tip of the device in PBS at 25°C (solid circles) and fluence from the tip (solid triangles). The concentration of pheophorbide was measured by fluorescence spectroscopy at the indicated times. The values shown here are an average of 3 or more measurements.

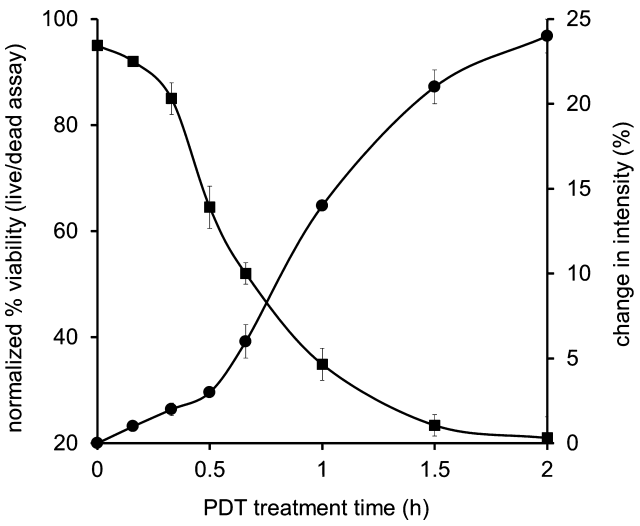

Figure 4. Time-sequence analysis of phototoxicity effects on U87 cells in 14 mm diameter microwell experiments treated with the device tip (solid squares) and fluence from the tip (solid circles). Cell viability was assessed by live/dead assay and results are shown as percent relative to control cells. Each value represents an average of two experiments.

the cell killing radius, where we placed the device tip 0.25 mm above U87 cells spread into a monolayer on a 200 μL microwell plate (diameter = 14 mm). Figure 5 shows the photokilling radius as a function of time. The nonviable, propidium iodide-stained detached cells were aspirated as part of the standard protocol for the live/dead assay. Consequently, the images in Fig. 5 show viable green attached cells. The radius of cell killing increases and proceeds from 0.1 to 2.9 mm for treatment times of 0.5 to 2.0 h, respectively. Compare the insets for "control" and treatment time = 0 h (Fig. 5), which shows that cell viability with only light and O_2 for 1 h is ~95% indicating that the sensitized formation of $^1O_2$ is required for the cell photokilling. A limited number of peripheral cell deaths were observed based on the fluorescence intensity of the attached cells from the no treatment image to those lying outside the treatment zones.

Mechanism

Our data support the mechanism depicted in Scheme 1. Visible light and oxygen gas emerge from the pointsource tip. The ethene group reacts with $^1O_2$ for sensitizer release, following dioxetane cleavage, availing the sensitizer's phototoxic activity to the U87 cells.

Notice there was an increased photokilling rate from 0.5 to 1.0 h (270 cells min^{-1}) relative to earlier 0 to 0.5 h (173 cells min^{-1}) or later in the reaction 1.0–2.0 h (182 cells min^{-1}). Thus, it follows the radius of cell killing increases in the midpoint of the reaction. The notion was the probe tip is most lethal at 0.5–1.0 h when the photorelease rate was at its fastest. We know as the result of work with native silica that using fluorinated silica increases the photorelease (26). In addition to a Teflon-like repellent surface, evidence is for reduced physical quenching of $^1O_2$ with the fluorinated silica compared to native silica (21), which is an important factor in the self-accelerated sensitizer release.

We view $^1O_2$ as a key species initiating events causing phototoxicity. Red-light irradiation of pheophorbides mainly proceeds by a Type-II (singlet oxygen) photosensitized mechanism (40,41) rather than a Type-I mechanism involving superoxide, hydroxyl radical and related species (42,43). It was evident from Fig. 2 that of the sensitizer delivered, ~20% diffused into the cells, but

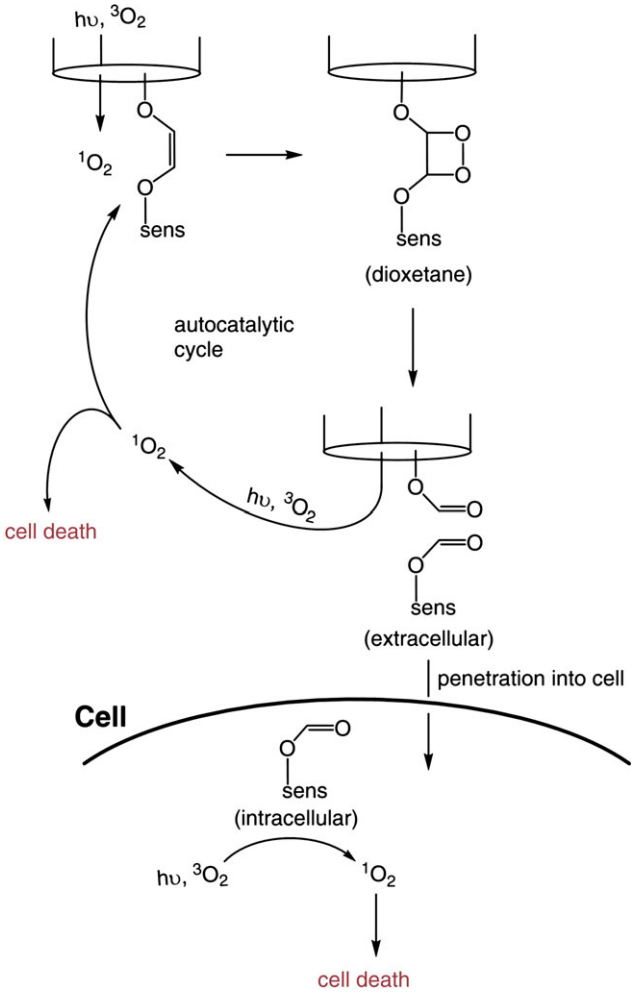

Scheme 1. Sensitizer drug and $^1O_2$ delivery and glioblastoma cell killing mechanism.

we did not discriminate whether cell death depends more on extracellular or intracellular $^1O_2$. Although an *inter*connection for the extracellular route could, in principle, be made with a

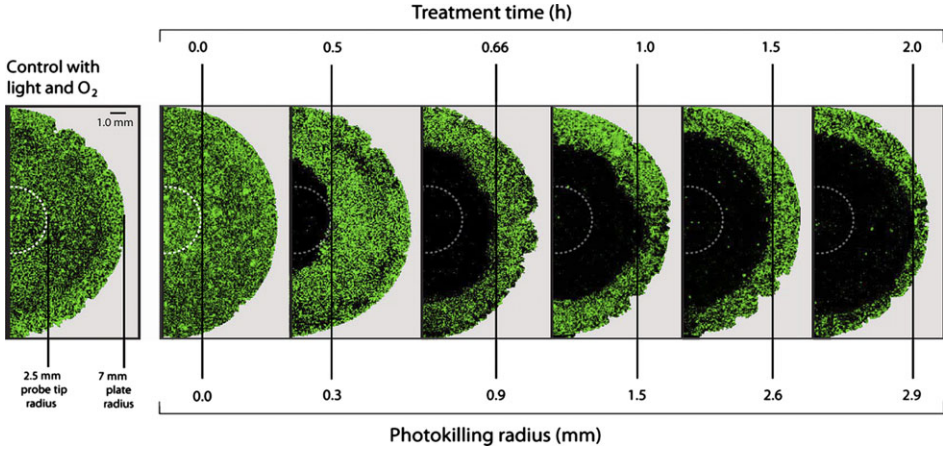

Figure 5. Device tip treatment of a U87 cell monolayer (154 mm^2 area) revealed a radius of photokilling as a function of time. Regions of the confocal fluorescence images show the probe tip radius in a white dashed line, the radius of photokilling and that of the plate edge. The cells were stained with calcein AM (green/live) for 30 min. Magnification 10×.

membrane-impermeable sensitizer (44). The diffusion coefficients of $^1O_2$ or of pheophorbide were not estimated due to the heterogeneity of the system.

CONCLUSION

We describe a microoptic device, which combines a diode laser, a hollow fiber optic and a porous silica probe tip, to deliver a pheophorbide (sensitizer) and singlet oxygen. The sensitizer photocleaves away from the probe tip and diffuses through media until it reaches the glioma cells. A rapid photorelease function was identified about midway through the reaction. This builds on the previous work that was published in 2013 (26), which found an autocatalytic-assisted photorelease of a sensitizer bound to a fluorosilane-coated silica surface into butanol and octanol solutions.

Development of the device for cancer eradication applications requires good precision in cell killing. Precision is important in treatment of cancers like glioma to minimize damage to critical normal nearby tissue (23,24). Additional experiments will grow from these initial experiments including optimization of sensitizer release, sensitizer cell uptake, light dose rates and also probe tip shape and surface conditioning to further enhance the cell killing. Our basic message is that the pointsource approach has potential benefits compared to conventional systemic photosensitizer delivery for PDT. Its significance may include the treatment of brain tumors, *e.g.* glioblastoma multiforme. That the device tip delivers $^3O_2$ is an essential (and somewhat indispensable) feature of the technique. The device can, in principle, connect to fiber optic methods to improve cell-killing precision in oxygen-poor sites during PDT (45).

Acknowledgements—A.A.G and A.G acknowledge support from the NIH-National Institute of General Medical Sciences (SC1GM093830). Grant support to I.R. and T.H. was provided by the NIH-National Cancer Institute (5R01CA160998). We thank Bryan Spring, Aki Palanisami, Huang-Chiao (Joe) Huang and Girgis Obaid for comments, and Leda Lee for the graphic arts work.

REFERENCES

1. Srivatsan, A., M. Ethirajan, S. K. Pandey, S. Dubey, X. Zheng, T.-H. Liu, M. Shibata, J. Missert, J. Morgan and R. K. Pandey (2011) Conjugation of cRGD peptide to chlorophyll *a* based photosensitizer (HPPH) alters its pharmacokinetics with enhanced tumor-imaging and photosensitizing (PDT) efficacy. *Mol. Pharmaceut.* **8**, 1186–1197.
2. Zhou, A., Y. Wei, B. Wu, Q. Chen and D. Xing (2012) Pyropheophorbide-*a* and c(RGDyK) comodified Chitosan-Wrapped upconversion nanoparticle for targeted near-infrared photodynamic therapy. *Mol. Pharmaceut.* **9**, 1580–1589.
3. Lim, C.-K., J. Shin, I. C. Kwon, S. Y. Jeong and S. Kim (2012) Iodinated photosensitizing chitosan: Self-assembly into tumor-homing nanoparticles with enhanced singlet oxygen generation. *Bioconjugate Chem.* **23**, 1022–1028.
4. Cui, Y., Y. Wu, Y. Liu, G. Yang, L. Liu, H. Fu, Z. Li, S. Wang and Y. Chen (2013) PEGylated nanoparticles of diperylene bisimides with high efficiency of $^1O_2$ generation. *Dyes Pigm.* **97**, 129–133.
5. Zhao, J., J. Fei, C. Du, W. Cui, H. Ma and J. Li (2013) Assembly of catalase-based bioconjugates for enhanced anticancer efficiency of photodynamic therapy in vitro. *Chem. Comm.* **49**, 10733–10735.
6. Dosselli, R., R. Ruiz-González, F. Moret, V. Agnolon, C. Compagnin, M. Mognato, V. Sella, M. Agut, S. Nonell, M. Gobbo and E. Reddi (2014) Synthesis, spectroscopic, and photophysical characterization and photosensitizing activity toward prokaryotic and eukaryotic cells of porphyrin-magainin and -buforin conjugates. *J. Med. Chem.* **57**, 1403–1415.
7. Cheng, Y., J. D. Meyers, A. Broome, M. E. Kenney, J. P. Basilion and C. Burda (2011) Deep penetration of a PDT drug into tumors by noncovalent drug-gold nanoparticle conjugates. *J. Am. Chem. Soc.* **133**, 2583–2591.
8. Cheng, Y., A. C. Samia, J. D. Meyers, I. Panagopoulos, B. Fei and C. Burda (2008) Highly efficient drug delivery with gold nanoparticle vectors for in vivo photodynamic therapy of cancer. *J. Am. Chem. Soc.* **130**, 10643–10647.
9. Wang, S., R. Gao, F. Zhou and M. Selke (2004) Nanomaterials and singlet oxygen photosensitizers: Potential applications in photodynamic therapy. *J. Mater. Chem.* **14**, 487–493.
10. Lacombe, S., J.-P. Soumillion, A. El Kadib, T. Pigot, S. Blanc, R. Brown, E. Oliveros, C. Cantau and P. Saint-Cricq (2009) Solvent-free production of singlet oxygen at the gas-solid interface: Visible light activated organic-inorganic hybrid microreactors including new cyanoaromatic photosensitizers. *Langmuir* **25**, 11168–11179.
11. Panagiotou, G. D., M. D. Tzirakis, J. Vakros, L. Loukatzikou, M. Orfanopoulos, C. Kordulis and A. Lycourghiotis (2010) Development of [60] fullerene supported on silica catalysts for the photo-oxidation of alkenes. *Appl. Catal. A* **372**, 16–25.
12. Ragas, X., A. Gallardo, Y. Zhang, W. Massad, C. D. Geddes and S. Nonell (2011) Singlet oxygen phosphorescence enhancement by silver islands films. *J. Phys. Chem. C* **115**, 16275–16281.
13. Mooi, S. M. and B. Heyne (2014) Amplified production of singlet oxygen in aqueous solution using metal enhancement effects. *Photochem. Photobiol.* **90**, 85–91.
14. Röder, B. (2000) *Photodynamic Therapy*. In *Encyclopedia of Analytical Chemistry* (Edited by A. Meyers), pp. 302–320. John Wiley & Sons, Chichester, UK.
15. Zamadar, M., G. Ghosh, A. Mahendran, M. Minnis, B. I. Kruft, A. Ghogare, D. Aebisher and A. Greer (2011) Photosensitizer drug delivery via an optical fiber. *J. Am. Chem. Soc.* **133**, 7882–7891.
16. Klán, P., T. Šolomek, C. G. Bochet, A. Blanc, R. Givens, M. Rubina, V. Popik, A. Kostikov and J. Wirz (2013) Photoremovable protecting groups in chemistry and biology: Reaction mechanisms and efficacy. *Chem. Rev.* **113**, 119–191.
17. Arian, D., L. Kovbasyuk and A. Mokhir (2011) 1,9-dialkoxyanthracene as a $^1O_2$-sensitive linker. *J. Am. Chem. Soc.* **133**, 3972–3980.
18. Hossion, A. M. L., M. Bio, G. Nkepang, S. G. Awuah and Y. You (2012) Visible light controlled release of anticancer drug through double activation of prodrug. *ACS Med. Chem. Lett.* **4**, 124–127.
19. Bio, M., P. Rajaputra, G. Nkepang, S. G. Awuah, A. M. L. Hossion and Y. You (2013) Site-specific and far-red-light-activatable prodrug of combretastatin A-4 using photo-unclick chemistry. *J. Med. Chem.* **56**, 3936–3942.
20. Komeda, C., A. Ikeda, J.-I. Kikuchi, N. Ishida-Kitagawa, H. Tatebe, K. Shiozaki and M. Akiyama (2013) A photo-triggerable drug carrier based on cleavage of PEG lipids by photosensitizer-generated reactive singlet oxygen. *Org. Biomol. Chem.* **11**, 2567–2570.
21. Bartusik, D., D. Aebisher, G. Ghosh, M. Minnis and A. Greer (2012) Fluorine end-capped optical fibers for photosensitizer release and singlet oxygen production. *J. Org. Chem.* **77**, 4557–4565.
22. Bartusik, D., D. Aebisher, A. Ghogare, G. Ghosh, I. Abramova, T. Hasan and A. Greer (2013) A fiberoptic (photodynamic therapy type) device with a photosensitizer and singlet oxygen delivery probe tip for ovarian cancer cell killing. *Photochem. Photobiol.* **89**, 936–941.
23. Mandel, S. and J. Glass (2009) Glioblastoma multiforme: Current treatment options and future directions. *Pract. Neurol.*, 16–19.
24. Eljamel, S. (2010) Photodynamic applications in brain tumors: A comprehensive review of the literature. *Photodiagnosis Photodyn. Ther.* **7**, 76–85.
25. Kandler, K., T. Nguyen, J. Noh and R. S. Givens (2013) An optical fiber-based uncaging system. *Cold Spring Harb. Protoc.* **8**, 118–121.
26. Bartusik, D., M. Minnis, G. Ghosh and A. Greer (2013) Autocatalytic-assisted photorelease of a sensitizer drug bound to a silica support. *J. Org. Chem.* **78**, 8537–8544.
27. Mahendran, A., Y. Kopkalli, G. Ghosh, A. Ghogare, M. Minnis, B. I. Kruft, M. Zamadar, D. Aebisher, L. Davenport and A. Greer (2011) A hand-held fiber-optic implement for the site-specific delivery of photosensitizer and singlet oxygen. *Photochem. Photobiol.* **87**, 1330–1337.

28. Merlin, J. L., S. Azzi, D. Lignon, C. Ramacci, N. Zeghari and F. Guillemin (1992) MTT assays allow quick and reliable measurement of the response of human tumour cells to photodynamic therapy. *Eur. J. Cancer* **28A**, 1452–1458.
29. De Mayo, P. (1982) Superficial Photochemistry. *Pure & Appl. Chem.* **54**, 1623–1632.
30. Bauer, R. K., R. Borenstein, P. de Mayo, K. Okada, M. Rafalska, W. R. Ware and K. C. Wu (1982) Surface photochemistry: Translational motion of organic molecules adsorbed on silica gel and its consequences. *J. Am. Chem. Soc.* **104**, 4635–4644.
31. Turro, N. J. (1987) Photochemistry of ketones adsorbed on porous silica. *Tetrahedron* **43**, 1589–1616.
32. Ottaviani, M. F., N. J. Turro, S. Jockusch and D. A. Tomalia (2003) EPR investigation of the adsorption of dendrimers on porous surfaces. *J. Phys. Chem. B* **107**, 2046–2053.
33. Jockusch, S., J. Sivaguru, N. J. Turro and V. Ramamurthy (2005) Direct measurement of the singlet oxygen lifetime in zeolites by near-IR phosphorescence. *Photochem. Photobiol. Sci.* **4**, 403–405.
34. Ramasamy, E., N. Jayaraj, M. Porel and V. Ramamurthy (2012) Excited state chemistry of capsular assemblies in aqueous solution and on silica surfaces. *Langmuir* **28**, 10–16.
35. Natarajan, A., L. S. Kaanumalle, S. Jockusch, C. L. D. Gibb, B. C. Gibb, N. J. Turro and V. Ramamurthy (2007) Controlling photoreactions with restricted spaces and weak intermolecular forces: exquisite selectivity during oxidation of olefins by singlet oxygen. *J. Am. Chem. Soc.* **129**, 4132–4133.
36. Greer, A. (2007) Organic chemistry: Molecular cross-talk. *Nature* **447**, 273–274.
37. Moan, J. (1990) On the diffusion length of singlet oxygen in cells and tissues. *J. Photochem. Photobiol. B* **6**, 343–344.
38. Feigenbaum, J. J., M. D. Choubal, D. S. Crumrine and J. R. Kanofsky (1996) Receptor inactivation by dye-neuropeptide conjugates: 2. Characterization of the quantum yield of singlet oxygen generated by irradiation of dye-neuropeptide conjugates. *Peptides* **17**, 1213–1217.
39. Hatz, S., L. Poulsen and P. R. Ogilby (2008) Time-resolved singlet oxygen phosphorescence measurements from photosensitized experiments in single cells: Effects of oxygen diffusion and oxygen concentration. *Photochem. Photobiol.* **84**, 1284–1290.
40. Röder, B., D. Naether, T. Lewald, M. Braune, C. Nowak and W. Freyer (1990) Photophysical properties and photodynamic activity in vivo of some tetrapyrroles. *Biophys. Chem.* **35**, 303–312.
41. Kuwabara, M., T. Yamamoto, O. Inanami and F. Sato (1989) Mechanism of photosensitization of pheophorbide-*a* studied by photohemolysis of erythrocytes and electron spin resonance spectrscopy. *Photochem. Photobiol.* **49**, 37–41.
42. Sauvaigo, S., T. Douki, F. Odin, S. Caillat, J.-L. Ravanat and J. Cadet (2001) Analysis of fluoroquinolone-mediated photosensitization of 2′-deoxyguanosine, calf thymus and cellular DNA: Determination of type-I, type-II and triplet-triplet energy transfer mechanism contribution. *Photochem. Photobiol.* **73**, 230–237.
43. Di Mascio, P., P. C. Teixeira, J. Onuki, M. H. G. Medeiros, D. Dornemann, T. Douki and J. Cadet (2000) DNA damage by 5-aminolevulinic and 4,5-dioxovaleric acids in the presence of ferritin. *Arch. Biochem. Biophys.* **373**, 368–374.
44. Pedersen, B. W., L. E. Sinks, T. Breitenbach, N. B. Schnak, S. A. Vinogradov and P. R. Ogilby (2012) Single cell responses to spatially controlled photosensitized production of extracellular singlet oxygen. *Photochem. Photobiol.* **87**, 1077–1091.
45. Busch, T. M. (2010) Hypoxia and perfusion labeling during photodynamic therapy. *Methods Mol. Biol.* **635**, 107–120.